



## Structural, Magnetic, and Transport Properties of $\text{LaMn}_{1-x}\text{Cu}_x\text{O}_3$ ( $x=0-0.125$ ) Ceramics

P. Kameli <sup>a</sup>, H. Vaezi <sup>a</sup>, M. H. Ehsani <sup>b\*</sup>, B. Aslibeiki <sup>c</sup>, H. Salamati <sup>a</sup>

<sup>a</sup> Department of Physics, Isfahan University of Technology, Isfahan, Isfahan, Iran

<sup>b</sup> Department of Physics, Semnan University, Semnan, Semnan, Iran

<sup>c</sup> Department of Physics, University of Tabriz, Tabriz, East Azerbaijan, Iran

### ARTICLE INFO

#### Article History:

Received 13 September 2020

Received in revised form 9 November 2020

Accepted 21 November 2020

#### Keywords:

Manganite Oxides

Doping

Spin Glass

Small Polaron Hopping

### ABSTRACT

The present study investigates the structural, magnetic, and electrical properties of non-stoichiometric  $\text{LaMn}_{1-x}\text{Cu}_x\text{O}_3$  ( $x=0, 0.025, 0.05, 0.075, \text{ and } 0.125$ ) ceramics. The results of X-ray diffraction refinement indicated that all samples were crystallized in an orthorhombic structure and no apparent crystal structure change was introduced by doping Cu up to  $x=0.125$ . The Ferromagnetic (FM) nature revealed by non-stoichiometric  $\text{LaMn}_{1-x}\text{Cu}_x\text{O}_{3-\delta}$  was verified through the appearance of Paramagnetic-Ferromagnetic (PM-FM) transition temperatures in AC magnetic susceptibility measurement of the samples. Due to the coexistence of Antiferromagnetic (AFM) and FM phases, all samples contained Re-entrant Spin Glass (RSG) and Cluster Spin Glass (CSG) states. The results showed that FM phase was comparable or even dominant in the doped samples up to  $x=0.075$ ; however, after doping, AFM phase overcame the FM phase as a result of reduction of double exchange interaction. Temperature dependence of resistivity measurement indicated that upon increasing the Cu-doping level, resistivity decreased, except for the  $x=0.125$  sample, and that metal-insulator transition at low temperatures was detected in the doped samples. Furthermore, changing the magnetic phase in the case of  $x=0.125$  sample from FM (in  $x=0.075$ ) to AFM dominant phase was accompanied by changing the transport parameters obtained from small polaron hopping models.

<https://doi.org/10.30501/acp.2021.233610.1044>

## 1. INTRODUCTION

Doped manganites  $\text{RMnO}_3$  ( $R=\text{rare-earth}$ ) with perovskite structures and a variety of magnetic and electrical behaviors have considerably attracted the attention of a number of researchers due to their remarkable coupling among freedom degrees of spin, charge, and orbit [1]. Manganese compounds can be applied in magnetic memory devices, sensors, refrigeration, medicine, biology, and photocatalytic activities [1-3].

Among these compounds, stoichiometric  $\text{LaMnO}_3$  ( $\text{LMO-La}^{3+}\text{Mn}^{3+}\text{O}_3$ ) is an A-type Antiferromagnetic (AFM) insulator below the Néel temperature ( $T_N$ ) of 140

K and the  $\text{Mn}^{3+}$  ions are coupled through a Super-Exchange (SE) interaction [4,5]. Besides the  $\text{ABO}_3$ -type perovskites, Manganese compounds of composition  $\text{AMnO}_3$  (Manganite) can be applied in magnetic memory devices, sensors, refrigeration, medicine, biology, and photocatalytic [4-6].

When a divalent  $\text{A}^{2+}$  ion such as ( $\text{A}=\text{Sr, Ca}$ ) is substituted for  $\text{La}^{3+}$  in  $\text{La}_{1-x}\text{A}_x\text{MnO}_3$  (LAMO), the  $\text{Mn}^{3+}/\text{Mn}^{4+}$  ratio changes. This mixed-valence of Mn ion allows an electron to hop between them and produce a Ferromagnetic (FM) Double-Exchange (DE) interaction, which also promotes metallic electrical conduction with different compositions,  $x$ , [6-8]. The complicated and fascinating magnetic, electrical, and structural properties of LAMO were attributed to strong coupling among spin,

\* Corresponding Author Email: [ehsani@semnan.ac.ir](mailto:ehsani@semnan.ac.ir) (M. H. Ehsani)

URL: [http://www.acerp.ir/article\\_127889.html](http://www.acerp.ir/article_127889.html)

Please cite this article as: Kameli, P., Vaezi, H., Ehsani, M. H., Aslibeiki, B., Salamati, H., "Structural, Magnetic and Transport Properties of  $\text{LaMn}_{1-x}\text{O}_3$  ( $x=0-0.125$ ) Ceramics", *Advanced Ceramics Progress*, Vol. 7, No. 1, (2021), 1-10. <https://doi.org/10.30501/acp.2021.233610.1044>



charge, orbital degrees of freedom, and lattice vibrations which were mainly explained by DE, Jahn-Teller (JT) distortion, and electron-phonon interactions. Besides the DE mechanism describing the interaction of  $Mn^{3+}$  and  $Mn^{4+}$  neighboring ions, JT distortion and electron-phonon interactions, phase separation, Griffiths phase, charge, and orbital ordering and their competitions, small polaron, and magnon correlated transport were employed to explain different properties of manganites [4-13]. As a result of a change in two effective parameters, i.e.,  $Mn^{3+}/Mn^{4+}$  ratio and angle/width of Mn-O-Mn bonds, in A-site doping, interesting magnetic and electrical properties are observed [14-21].

In addition to this kind of doping, the Mn-site doping with magnetic or nonmagnetic ions also offers numerous attractive properties for manganites. Experimental studies on B-site doping in stoichiometric polycrystalline  $LaMn_{1-x}B_xO_3$  (LMBO) compound by magnetic cations (B= Fe, Co, Ni, Cr, ...) and nonmagnetic cations (B=Zn, Li, Ga, Ti, ...) have demonstrated different physical properties, due to the concurrence of different valence states of Mn ions and magnetic interaction between the magnetic substituted ions and Mn ions [22-31]. De Lima et al. [22] investigated the magnetic properties of  $LaMn_{1-x}Fe_xO_{3+\delta}$  ( $0 \leq x \leq 1$ ) samples and detected some signs of the occurrence of CG in the whole doping range as well as appearance of FM phase and suppression of ferromagnetism while x increased. Sun et al. [23] and Ramos et al. [24] reported that Cr-doping in the LMO samples introduced ferromagnetism and CG behavior. Gong et al. [25] and Tong et al. [26] studied magnetic, electrical, and magneto-transport properties of Zn-doped LMO samples. Focusing on Jahn-Teller effects on FM nature, PM-FM phase, MR behavior, and carrier transport mechanism, they found that Zn-doping could decrease the effects of Jahn-Teller distortion and observed CG behavior. Shana et al. [27] observed an RSG state for Ti-doped LMO samples. Hebert et al. [28] reported the effects of Co, Ni, Zn, Li, and Ga-doping in the LMO samples in detail and showed that establishment of ferromagnetism and enhancement of conductivity in all samples strongly depended on the valence of doping ions and, consequently, the  $Mn^{3+}/Mn^{4+}$  ratio.

Knizek et al. [29] studied the structural, electro-magnetic, and catalytic characterization of the  $LaMn_{1-x}Cu_xO_{3+\delta}$  ( $x=0, 0.05, 0.10, 0.25, 0.5, 0.75, 0.90$  and  $0.95$ ) samples prepared by the solid-state reaction method with different preparation procedures (slowly cooled and quenched samples). Different properties of those samples were reported.

This paper intended to obtain a comprehensive experimental characterization of the intermediated doped  $LaMn_{1-x}Cu_xO_{3+\delta}$  ( $x=0, 0.025, 0.05, 0.075, \text{ and } 0.125$ ) samples prepared by a simple method, including novel results of AC magnetic susceptibility and resistivity versus temperature measurements.

## 2. EXPERIMENTAL PROCEDURE

The  $LaMn_{1-x}Cu_xO_{3+\delta}$  ( $x= 0, 0.025, 0.05, 0.075, \text{ and } 0.125$ ) samples were prepared through a simple synthesis method which was based on grinding the acetate precursors in the presence of citric acid [32]. The synthesis process is briefly summarized in the following: first, manganese acetate, lanthanum acetate, copper acetate, and citric acid powders were mixed by an equal molar ratio of total metal acetates to citric acid. Then, the powders were ground for 2 h and the ground powders were annealed in the air at  $600^\circ\text{C}$  for 6 h. Next, the annealed powders were palletized under pressure of  $10^5 \text{ N/cm}^2$  and sintered at  $1200^\circ\text{C}$  for 6 h. The resistivity measurements were carried out by the four-probe method using a Leybold closed-cycle refrigerator. The AC susceptibility measurements were performed using a Lake Shore AC Susceptometer (Model 7000). Finally, the X-Ray Diffraction (XRD) patterns of the samples were taken on Philips XPERT X-ray diffractometer.

## 3. RESULTS AND DISCUSSION

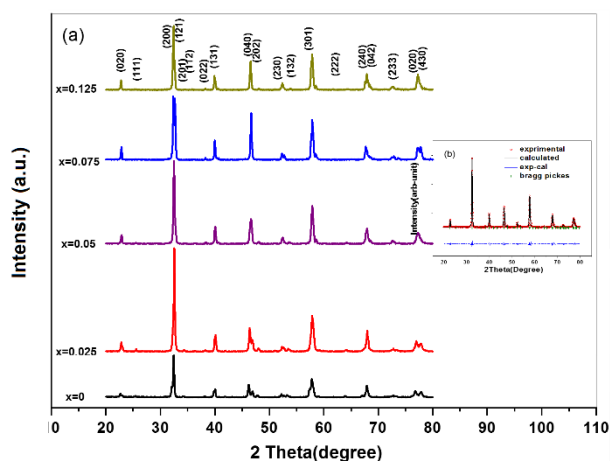
### 3.1. STRUCTURAL PROPERTIES

Figure 1 shows XRD patterns for all samples. The XRD data were analyzed by Rietveld refinement using the FULLPROF program, the results of which are collected in Table 1. A typical diagram for Rietveld refinement analysis of  $x=0.025$  sample is shown in Figure 1(b), which is indicative of a good agreement between the observed and calculated profiles. According to this analysis, no trace of secondary phase was detectable and the samples had an orthorhombic crystal structure with Pbnm space group.

Based on the data collected in Table 1, in case the x value changed from  $x=0$  to 0.05 (first group), the unit cell volumes of the samples would slightly increase; however, these volumes decreased for  $x=0.075$  and  $x=0.125$  samples (second group).

The obtained results for the first group was already expected. Since the Cu ions with a stable form of  $Cu^{2+}$  [32, 33] have larger ionic radii ( $0.73 \text{ \AA}$ ) than the average ionic radii of Mn ( $Mn^{3+} = 0.65 \text{ \AA}$  and  $Mn^{4+} = 0.53 \text{ \AA}$ ) [27], the substitution of  $Cu^{2+}$  would systematically increase the bond length, lattice parameters, and unit cell volumes. However, the uncommon decreasing behavior in the unit cell volume of  $x=0.075$  and  $x=0.125$  samples suggests that some of the substituted Cu ions are in a  $Cu^{3+}$  state with a radius of  $0.54 \text{ \AA}$ , which is smaller than that of  $Mn^{3+}$  and larger than that of  $Mn^{4+}$  [34]. Therefore,  $Cu^{3+}$  and  $Cu^{2+}$  states may appear in these samples, suggesting that the changes of the unite cell volume and lattice parameters are not regular with Cu content.

A similar phenomenon was observed in  $(\text{La,Ba})\text{Cu}_{1-x}\text{Mn}_x\text{O}_3$  and  $\text{La}_{0.7}\text{Sr}_{0.3}\text{Mn}_{1-x}\text{Cu}_x\text{O}_3$  compounds, where  $\text{Cu}^{3+}$  ions were substituted for the Mn ions sites [35,36].



**Figure 1.** (a) XRD patterns for all samples, (b) Room temperature XRD pattern (red symbol) and Rietveld profile file (black line) for  $x=0.025$  sample

**TABLE 1.** Lattice parameters (a and c), unit cell volume (V), average crystallite size, and (D) grain size

Sample Name	a (Å)	b (Å)	c (Å)	V (Å <sup>3</sup> )
$x=0.00$	5.521(3)	5.432(6)	7.847(2)	235.376(9)
$x=0.025$	5.544(7)	5.397(1)	7.365(5)	235.513(1)
$x=0.050$	5.527(8)	5.450(6)	7.835(9)	235.673(2)
$x=0.075$	5.557(1)	5.373(6)	7.839(7)	234.100(1)
$x=0.125$	5.538(3)	5.393(2)	7.833(6)	233.986(1)

### 3.2. MAGNETIC PROPERTIES

Figures 2- 4(a) show the real ( $\chi'$ ) and imaginary ( $\chi''$ ) parts of AC susceptibility for the samples that were measured in the AC field of 10 Oe and frequencies of 40, 111, 333, 666, and 1000 Hz, respectively.

Two peaks in the curves of AC susceptibility of the parent sample were observed upon decreasing the temperature, as shown in Figure 2(a). The sharp peak with a  $\lambda$ -shaped character was also observed at lower temperatures known as the Neel temperature, i.e.,  $T_N$ , a frequency-independent temperature repeatedly observed for stoichiometric LMO samples between 100 and 140K [4, 5]. The broad peak observed in AC magnetic susceptibility curves might be related to Curie temperature.

While the stoichiometric LMO has AFM nature, non-stoichiometric LMO which easily adopts excess oxygen shows a different magnetic phase diagram [32, 37]. In

fact, in the non-stoichiometric compound  $\text{LaMnO}_{3+\delta}$ , excess oxygen changes some of the  $\text{Mn}^{3+}$  ions to  $\text{Mn}^{4+}$  ions, thus leading to the charge imbalance in the lattice and, consequently, FM-DE interactions between  $\text{Mn}^{3+}$  and  $\text{Mn}^{4+}$  ions. In the magnetic phase diagram of  $\text{LaMnO}_{3+\delta}$ , both FM insulator and FM clusters embedded in an AFM matrix were observed depending on the values of  $\delta$  [32, 37].

Therefore, the second peak observed in the curves of AC magnetic susceptibility (Fig.2(a)) at higher temperatures could be related to Curie temperature transition ( $T_C \sim 167\text{K}$ ); accordingly, the parent sample was considered non-stoichiometric  $\text{LaMnO}_{3+\delta}$ .

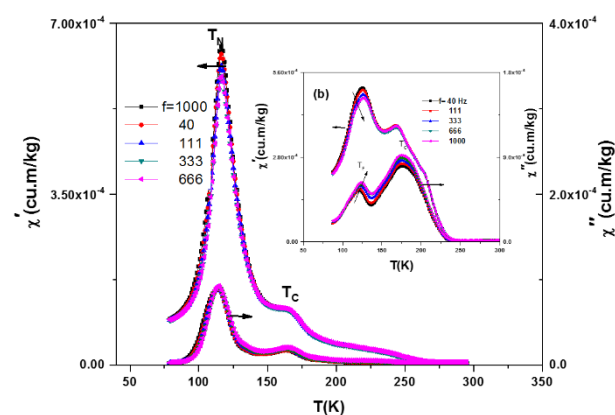


**Figure 2.** (a) Temperature dependence of left)  $\chi'$  and right)  $\chi''$  for  $x=0$  in a magnetic field of 10 Oe and frequencies of 40, 111, 333, 666, and 1000 Hz, (b) Temperature dependence of left)  $\chi'$  and right)  $\chi''$  for  $x=0.025$  in a magnetic field of 10 Oe and frequencies of 40, 111, 333, 666, and 1000 Hz

Joy et al. compared the Curie temperatures of  $\text{LaMnO}_{3+\delta}$  compound and regarded them as a function of  $\text{Mn}^{4+}$  content from the related literature. They found that the Curie temperature of non-stoichiometric  $\text{LaMnO}_{3+\delta}$  depended on the synthesis method or growth conditions such as calcination/sintering temperatures and could change from 60K to 280K [25]. A comparison of the values of Curie temperature ( $T_C \sim 167\text{K}$ ) obtained from the susceptibility magnetic measurement with those of other reports [32] confirmed that  $\delta \leq 0.11$  in the present sample.

Similar to the parent sample, two peaks were observed in the patterns of AC magnetic susceptibility of other samples as well. Figures 2(b)-4(a) show that Curie temperatures  $T_C$  become sharper and increase with the Cu content growth. The  $\text{Cu}^{2+}$  substitution on Mn sites produces the  $\text{Mn}^{4+}$  ions to maintain the electroneutrality of the lattice. Accordingly, upon increasing the  $\text{Mn}^{4+}/\text{Mn}^{3+}$  ratio, the local DE between  $\text{Mn}^{3+}$  and  $\text{Mn}^{4+}$  would be developed in the  $\text{Mn}^{3+}\text{-O-Mn}^{3+}$  AFM background. Therefore, the peak corresponding to Curie

temperature for  $x=0.025$  to  $x=0.075$  samples (Fig.3 (b)) became considerably sharper. In the case of  $x=0.075$  sample, the proportion of DE within the framework of the  $Mn^{3+}$ -O- $Mn^{4+}$  interaction overwhelmed the AFM SE interactions of  $Mn^{3+}$ -O- $Mn^{3+}$  and  $Cu^{2+}$ -O- $Cu^{2+}$  networks. However, as depicted in Figure 4(a), the pattern of AC susceptibility indicates that while the proportion of DE decreases with further doping of Cu in  $x=0.125$  sample, that of the  $Cu^{2+}$ -O- $Cu^{2+}$  or  $Cu^{3+}$ -O- $Cu^{3+}$  AFM interactions increases, thus decaying the macroscopic ferromagnetism in this sample. The same behavior was reported by Sun et al. in  $LaMn_{1-x}Cu_xO_3$ , but for  $x=0.3$  sample [28]. Such difference was observed probably due to the  $Mn^{4+}/Mn^{3+}$  ratio in the crystal lattice of samples, which strongly depended on the oxygen stoichiometry [33].

Contrary to what is seen in Figure 2(a), for the first peak at a lower temperature for the parent sample, all the doped samples showed a frequency-dependent peak ( $T_f$ ).  $T_f$  shifted towards higher temperature by increasing the frequency, thus confirming the coexistence and competition between FM and AFM interactions and favoring the formation of a spin/cluster glass states. Similar behavior was also identified by substituting Mn for Fe, Ti, Ga, Cr, and other cations in manganites [22, 38-40]. Such frequency-dependent behavior can be normally related to the existence of Spin-Glass(SG) or CG phases in these samples.

Based on the experimental data obtained from the frequency dependence of freezing temperature,  $T_f$ , can be expressed through the conventional Critical Slowing Down (CSD) model [41, 42]:

$$f = f_0 \left( \frac{T_f - T_g}{T_g} \right)^{zv} \quad (1)$$

where  $f_0$  is in the range of  $10^9$ - $10^{13} s^{-1}$  for SG systems,  $T_g$  is the RSG transition temperature, and  $T_f$  is the frequency-dependent freezing temperature, at which the maximum relaxation time of the system corresponds to the measured frequency. Parameter  $zv$  is a dynamic critical exponent which shows the strength of interactions and varies between 4 and 12 for SG systems.

The Ln-Ln plot of the external frequency ( $f$ ) versus reduced temperature,  $(T_f - T_g)/T_g$ , shows an excellent linear dependence, as depicted in Fig. 4(b). The best-fitting values are given in Table 2. The estimated values for  $x=0.025$  and  $x=0.05$  samples were within the realm of three-dimensional spin-glasses [43]. RSG behavior was found in a variety of disordered magnetic materials, in which there was a competition between SG ordering and long-range FM ordering, i.e., in the systems with a majority of FM couplings between the individual spins and a sufficiently large number of AFM couplings, to create substantial frustration. In case of a decrease in the temperature, this system shows a transition from PM to

FM phases. Upon further reduction of the temperature, typical SG behavior, commonly called RSG, is observable. By substituting Cu for Mn, the density of the holes ( $Mn^{4+}$ ) would increase and the DE interaction would be improved. Any increase in the  $Mn^{4+}$  and FM phase in AFM matrix would produce spin frustration and cause the occurrence of RSG in  $x=0.025$  and  $x=0.05$  samples. In the case of  $x=0.075$ , Cu content was sufficient to improve the long-range FM ordering with a CG regime at low temperatures. Therefore, the values given in Table 2 are out of the predicted values for the SG system. Moreover, in the case of  $x=0.125$ , AFM ordering is dominant and the estimated  $zv$  value is out of the predicted values for SG systems.

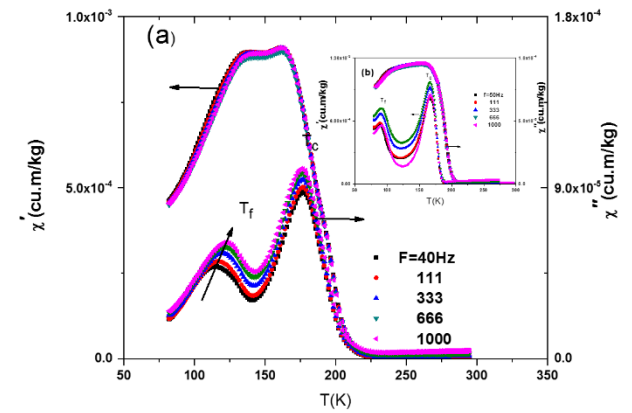


**Figure 3.** Temperature dependence of left)  $\chi'$  and right)  $\chi''$  for  $x=0.05$  in a magnetic field of 10 Oe and frequencies of 40, 111, 333, 666, and 1000 Hz, (b) Temperature dependence of left)  $\chi'$  and right)  $\chi''$  for  $x=0.075$  in a magnetic field of 10 Oe and frequencies of 40, 111, 333, 666, and 1000 Hz

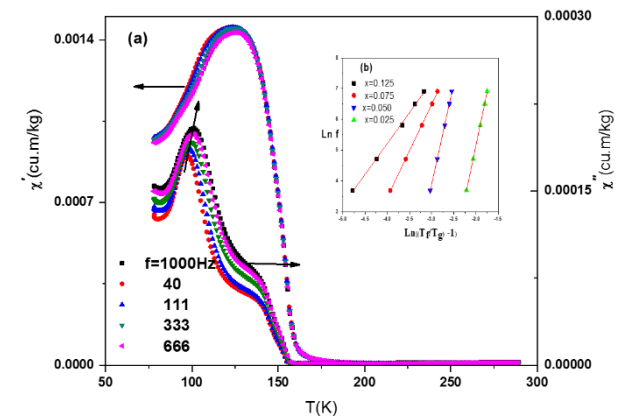


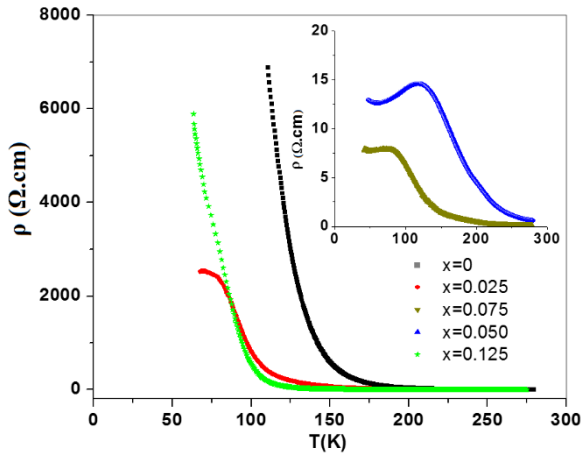
**Figure 4.** Temperature dependence of left)  $\chi'$  and right)  $\chi''$  for  $x=0.125$  in a magnetic field of 10 Oe and frequencies of 40, 111, 333, 666, and 1000 Hz, (b) Ln-Ln plot of the reduced temperature  $(T_f/T_g - 1)$  versus frequency for all samples

**TABLE 2.** Parameters obtained from analysis of the experimental data using CSD model

Sample	$T_c$ (K)	Zv	$f_0$ (s <sup>-1</sup> )	$T_g$ (K)
x=0	164		-	-
x=0.025	176	6.88	$\sim 10^{10}$	120
x=0.050	177	6.58	$\sim 10^9$	114
x=0.075	178	3.01	$\sim 10^7$	93
x=0.125	140	2.00	$\sim 10^{10}$	93

### 3.3. ELECTRICAL PROPERTIES

Electrical transport properties of the samples were systematically studied. Figure 5 shows the temperature dependence of resistivity for the samples.

**Figure 5.** Temperature dependence of resistivity for the samples  $\rho$  ( $\Omega$ .cm)

As observed, the parent sample ( $x=0$ ) was an insulator in the whole measuring temperature. Upon increasing the doping level, the resistivity of all the samples would decrease and the curves of the temperature dependence of resistivity showed Metal-Insulator (MI) transition, except for  $x=0.125$  sample. The resistivity of  $x=0.075$  sample was almost the third order of magnitude smaller than the  $x=0$  sample. This kind of behavior can be justified by the percolation model [39]. Of note, there were an FM- DE interaction between  $Mn^{3+}$  and  $Mn^{4+}$  neighboring ions and an AFM- SE interaction between  $Mn^{3+}$  ions in the Perovskite manganites. While the FM interaction caused metallic behavior, the AFM interaction instigated insulating behavior. As mentioned earlier, the parent compound  $LaMnO_3$  was the AFM insulator, in which doping of Cu ion in Mn ion site and excess oxygen would lead to enhancement of the  $Mn^{4+}$  ions ratio and consequently, the DE interaction and ferromagnetism. Moreover, an increase in the Cu content

and excess oxygen would form FM clusters in the AFM matrix. Therefore, short-range ordering in the clusters would gradually increase to long-range ordering. For the un-doped sample, due to the low degree levels of  $Mn^{4+}$  ions, the FM clusters were separated and the volume of the FM clusters did not reach the percolation threshold. Therefore, the system exhibited a high-resistance and insulating behavior. As temperature decreased in Cu-doped samples to  $x=0.075$  sample, the FM component increased and a percolation channel was formed due to the high levels of  $Mn^{4+}$  ions, hence a decrease in the resistivity and occurrence of the MI transition. In the case of  $x=0.125$  sample, the substituted Cu for Mn sites formed an  $Mn^{3+}$ -O-Cu<sup>2+</sup>/Cu<sup>3+</sup>-Mn<sup>4+</sup> bonds which could create a potential barrier for charge carriers to hop. Therefore, at this level of doping, the MI transition would disappear.

To investigate the transport mechanism that can describe the temperature dependence of the resistivity of samples, the resistivity data of samples in the semiconducting region were selected and fitted by common models, namely Mott's Variable-Range Hopping (VRH) and Mott and Davis's Small Polaron Hopping (SPH) models [44, 45].

In Mott's VRH model, the transport mechanism is described as follows [46]:

$$\rho = \rho_0 \exp\left(\frac{T_0}{T}\right)^{1/4} \quad (2)$$

where  $T_0$  is Mott characteristic temperature which is given by:

$$T_0 = \frac{18}{k_B N(E_F) a^2} \quad (3)$$

where  $N(E_F)$  is the Density of States (DOS) near the Fermi level,  $k_B$  is Boltzmann's constant, and  $a$  parameter is the localization length.

The mean hopping distance,  $R_h(T)$ , and hopping energy,  $E_h(T)$ , can be obtained at a given temperature  $T$ , as expressed in the following equations [47]:

$$R_h(T) = \frac{3}{8} a \left(\frac{T_0}{T}\right)^{1/4} \quad (4)$$

$$E_h(T) = \frac{1}{4} k_B T^{1/4} T_0^{1/4} \quad (5)$$

The present resistivity data were fitted using Mott's VRH model to evaluate parameters  $\rho_0$  and  $T_0$ . Figure 6(a) demonstrates the typical fitting analysis by comparing the experimental data and the model for  $x=0$  and 0.025 samples.

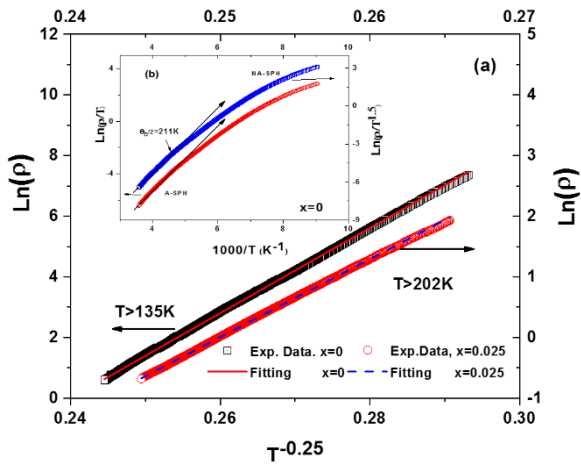


**Figure 6.** (a) Plot of  $\text{Ln}(\rho)$  versus  $T^{-0.25}$  at different temperature regions (open symbols and lines represent the experimental data and fitting result, respectively,  $x=0$  and  $x=0.025$  samples) (b) Plots of  $\text{Ln}(\rho/T)$  and  $\text{Ln}(\rho/T^{3/2})$  versus  $(1/T)$  for the sample  $x=0$

The plot revealed a good correlation between the data and model in different ranges of temperature, i.e., temperatures more than 135, 202, 217, 200, and 100K for  $x=0, 0.025, 0.05, 0.075,$  and  $0.125$  samples, respectively, suggesting the presence of two different valent transition–metal elements (Mn and Cu) in lattice-affected and electronic properties of a system due to the change in hopping conditions for charge carrier and induced distortion effects.

By considering the obtained values of  $T_0$  from the fitted results,  $N(E_F)$ ,  $R_h$ , and  $E_h$  were estimated at different temperatures of 100, 150, and, 300K (see Table 3) through taking the localization length of  $a=4.5 \text{ \AA}$ , as reported for such materials [48].

**TABLE 3.** Values of  $N(E_F)$ ,  $R_h$ , and  $E_h$  at room temperature

Sample	$R^2$	$\rho_0(\Omega \cdot \text{cm})$	$T_0$	$N(E_F)(\text{eV}^{-1}\text{m}^{-3}) \times 10^{24}$	$R_h(300\text{K}) (\text{\AA})$	$E_h(300\text{K}) (\text{meV})$
$x=0$	0.99958	$2.12 \times 10^{-15}$	$3.98 \times 10^8$	5.84	57.06	218.5
$x=0.025$	0.99971	$1.08 \times 10^{-14}$	$2.73 \times 10^8$	8.39	52.16	199.8
$x=0.05$	0.99936	$1.2 \times 10^{-11}$	$1.02 \times 10^8$	22	40.75	156.12
$x=0.075$	0.9940	$2.58 \times 10^{-11}$	$6.02 \times 10^7$	38	35.71	136.81
$x=0.125$	0.9963	$1.66 \times 10^{-13}$	$1.52 \times 10^8$	15	45.08	172.69

According to Table 3, by increasing the Cu-doping level, the density of states at the Fermi level increases, which corresponds to an increase in conductivity. Therefore, substitution of Cu for Mn ion sites could increase the  $\text{Mn}^{4+}/\text{Mn}^{3+}$  ratio and, in this condition, the

charge carriers would better hop between the  $\text{Mn}^{3+}$  to  $\text{Mn}^{4+}$  sites through DE mechanism. A decrease in the hopping distance ( $R_h$ ) and hopping energy ( $E_h$ ) of charge carrier obtained from the transport model confirmed the improvement of hopping conditions and accordingly, in the parent sample,  $e_g$  electrons of  $\text{Mn}^{3+}$  were more localized and, in the doped samples, the effective DE interaction between  $\text{Mn}^{3+}\text{-Mn}^{4+}$  became stronger.

The data for  $x=0.125$  sample obtained from fitting showed a different behavior from those of other samples. As expected from the magnetic data analysis, in this sample, the formation of  $\text{Mn}^{3+}\text{-O-Cu}^{2+}/\text{Cu}^{3+}\text{-Mn}^{4+}$  bonds decreased the connection channel and considerably increased charge carrier hopping distance, thus decreasing conductivity.

Another attempt was also made to confirm the nature of hopping conduction and the strength of electron–phonon interaction. The conduction mechanism for manganites at high temperatures,  $T > \theta_D/2$  ( $\theta_D$  is Debye's temperature) was mainly due to the thermally activated small polarons. The polaronic models are either adiabatic or non-adiabatic approximations. In the adiabatic regime, the nearest neighboring hopping of small polarons (Holstein polarons) leads to mobility with a thermally activated form, in which charge-carrier motion is faster than lattice vibrations. In the non-adiabatic regime, it is the opposite. According to these mechanisms, the temperature dependence of resistivity ( $\rho$ ) is expressed as follows [48]:

$$\rho = \rho_\alpha T \exp\left(\frac{E_a}{K_B T}\right) \quad (\text{adiabatic}) \quad (6)$$

$$\rho = \rho_\alpha T^{3/2} \exp\left(\frac{E_a}{K_B T}\right) \quad (\text{non-adiabatic}) \quad (7)$$

where  $E_a$ ,  $\rho_\alpha$ , and  $K_B$  are activation energy, residual resistivities, and Boltzman's constant, respectively.

Conduction can occur in either adiabatic or non-adiabatic models. Therefore, through Equations (6) and (7), the  $\text{Ln}(\rho/T)$  and  $\text{Ln}(\rho/T^{3/2})$  versus  $(1/T)$  plot was separately drawn for the samples. Figure 7 shows the typically related plots for  $x=0$  and  $0.05$ . Within all temperature ranges of measurements, Debye's temperature for the samples was estimated from the plots of  $\text{Ln}(\rho/T)$  and  $\text{Ln}(\rho/T^{3/2})$  versus  $(1000/T)$ . The value of  $\theta_D/2$  was considered to be the deviation point from linearity in the low-temperature region [49-53]. The obtained values of  $\theta_D$  were calculated as 430, 442, 432, 400, and 310K for  $x=0, 0.025, 0.050, 0.075,$  and  $0.125$  samples, respectively, which were close to the previously reported values for similar compounds [52, 53].

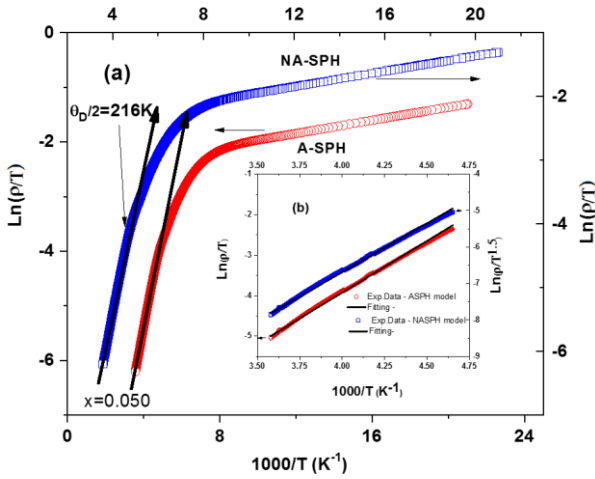


**Figure 7.** Plots of  $\ln(\rho/T)$  and  $\ln(\rho/T^{3/2})$  versus  $(1/T)$  for the sample  $x=0.05$  (b) Plots of experimental data of the sample  $x=0$  (with adiabatic small polaron hopping (ASPH) and non-adiabatic small polaron hopping (NASPH) models)

The data of the high temperature just above Debye's temperatures ( $\theta_D/2$ ) were selected to study the transport regime and fitted by adiabatic and non-adiabatic models. Figure 8 shows the related plots for  $x=0$  and  $x=0.05$ . The obtained parameters are given in Table 4. As observed in the data collected in Table 4, the linear correlation coefficients,  $R^2$ , for the samples were very close to 1 and were almost the same for both models. Therefore, it was difficult to identify the nature of the hopping mechanism in this temperature range by this analysis.

In order to find how the carriers hop, i.e., adiabatic or non-adiabatic hopping, in this temperature range, the necessary conditions for using either of these mechanisms should be checked. Holstein's relation can help distinguish the kind of hopping mechanism [49]. It can be suggested that  $J$  (polaron bandwidth) can be treated as a perturbation in the corresponding Schrödinger equation. According to Holstein's condition,  $J$  should satisfy the inequality  $J > \phi$  for adiabatic hopping and  $J < \phi$  for non-adiabatic hopping conduction, where  $\phi$  is:

$$\phi = \left(\frac{2k_B T E_a}{\pi}\right)^{1/4} \left(\frac{h\nu}{\pi}\right)^{1/2} \quad (8)$$

Moreover, the condition for small-polaron formation is  $J < E_a/3$  [49]; otherwise, there will be large polarons.

The value of  $J$  can be estimated by approximating the equation for high-temperature jump site [51, 52]:

$$J \cong 0.67 h \nu_{ph} \left(\frac{T}{\theta_D}\right)^{1/4} \quad (9)$$

In this evaluation,  $\nu_{ph}$  was estimated to be about  $10^{13}$  Hz from the relation  $h\nu_{ph} = k_B \theta_D$  (see Table 4) and  $T=200$  and  $300$  K. Since  $J < \phi$  and  $J < E_a/3$  for all the samples, it

can be concluded that the non-adiabatic small polaron hopping model was responsible for conduction in all samples in this temperature range.

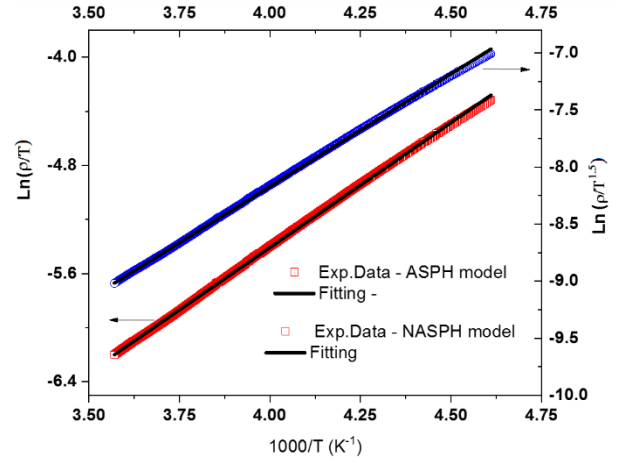


**Figure 8.** Plots of experimental data of the sample  $x=0.05$  (with adiabatic small polaron hopping (ASPH) and non-adiabatic small polaron hopping (NASPH) models)

It is interesting to estimate a few important relevant physical parameters for compounds. The values for small-polaron coupling ( $\gamma_p$ ), which is a measure of electron-phonon interaction in these manganites, can be evaluated from the following relation:

$$\gamma_p = 2E_a/h\nu_{ph} \quad [54,55].$$

In addition, the polaron mass ( $m_p$ ) and rigid lattice effective mass ( $m^*$ ) in the manganites were related by the following equation [54]:

$$m_p = \left(\frac{h^2}{8\pi^2 J a_p}\right) \exp(\gamma_p) = m^* \exp(\gamma_p) \quad (10)$$

The calculated values for  $\gamma_p$  and  $m_p/m^* = \exp(\gamma_p)$  are collected in Table 4 that shows a decrease in the  $\gamma_p$  and  $m_p/m^*$  values for the doped samples. If the value of  $\gamma_p$  is greater than 4, there are strong electron-phonon (e-ph) interaction in the system; otherwise, the interactions are weak [51, 54].

According to Table 4, the values of the present samples were found to be more than 4, thus confirming the strong e-ph interactions in the compounds and ensuring the formation of polarons. Moreover, as the Cu concentration increased, the strength of the e-ph coupling constant systematically decreased, which resulted in the creation of the  $Mn^{4+}$  ions in the doped samples and improvement of DE interaction. The reduction of e-ph coupling stopped in the case of  $x=0.125$  sample. Analysis of the transport properties of the samples showed that distortion of the unit cell causing the JT effect decreased and this effect was suddenly weakened in  $x=0.125$  sample, which could be closely correlated to structural and magnetic analyses.

**TABLE 4.** Some important estimated parameters related to ADSPH and NADSPH models

Sample	$\theta_D$ (K)	$v_{Ph} \times 10^{-13}$	ADSPH-Model		NADSPH-Model		$\phi$ (meV)		J (meV)		$\gamma_p$	$m_p/m$
			$R^2$	$E_p$ (meV)	$R^2$	$E_p$ (meV)	At	At	At	At		
							T=200K	T=300K	T=200K	T=300K		
x=0	430	0.84	0.9975	220	0.9974	231	23.32	25.8	19.29	21.34	11.9	147.3
x=0.025	442	0.92	0.99911	199	0.99912	210	23.79	26.31	20.94	23.16	10.4	34.2
x=0.050	432	0.90	0.99983	159	0.99982	170	22.24	24.6	20.57	22.76	8.5	5.0
x=0.075	400	0.83	0.9981	138	0.9984	149	20.66	22.85	19.41	21.47	8.0	3.0
x=0.125	310	0.64	0.99989	146	0.99981	155	18.45	20.41	16.01	17.74	11	59.8

#### 4. CONCLUSION

In this paper, the effect of Cu doping on  $\text{LaMn}_{1-x}\text{Cu}_x\text{O}_{3+\delta}$  ( $x=0-0.125$ ) manganite material was investigated. The results of powder X-ray diffraction indicated that the samples were single-phased and crystallized in an orthorhombic structure with Pbnm space group. Enhancement in the unit cell volumes of the doped samples to  $x=0.050$  was systematical. However, after the maximum of 7.5% substitution of Cu, a decrease in the unit cell volumes was observed. Any uncommon decrease in the unit cell volume of  $x=0.075$  and  $x=0.125$  samples could be a result of the appearance of Cu ions as  $\text{Cu}^{3+}$  state in this sample. The PM-FM transition temperature,  $T_c$ , increased when the Cu content increased. RSG state accompanied by FM transition existed in  $x=0.025$  and  $x=0.05$  samples. By substituting Cu for Mn, the density of the holes ( $\text{Mn}^{4+}$ ) increased and the DE interaction was improved. An increase in the DE interaction and FM phase in AFM matrix produced spin frustration and RSG in  $x=0.025$  and  $x=0.05$  samples. In the  $x=0.075$  sample, the FM ordering was observed and the magnetic data analysis based on the critical slowing model confirmed the CS state in this sample. After 7.5% doping in the Mn site by Cu, the AFM phase overcame the FM phase due to the reduction of DE interaction. Investigation of the electrical behavior based on VRH and polaronic transport models was performed according to the structural and magnetic measurement analyses.

#### ACKNOWLEDGEMENT

The authors would like to thank Isfahan University of Technology for supporting this project.

#### REFERENCES

- Jin, S., Tiefel, T. H., McCormack, M., Fastnacht, R. A., Ramesh, R., Chen, L. H., "Thousandfold change in resistivity in magnetoresistive La-Ca-Mn-O films", *Science*, Vol. 264, No. 5157, (1994), 413-415. <https://doi.org/10.1126/science.264.5157.413>
- Asamitsu, A., Moritomo, Y., Tomioka, Y., Arima, T., Tokura, Y., "A structural phase transition induced by an external magnetic field", *Nature*, Vol. 373, No. 6513, (1995), 407-409. <https://doi.org/10.1038/373407a0>
- Tokura, Y., Ed., *Colossal Magnetoresistive Oxides*, CRC Press, (2000). <https://doi.org/10.1201/9781482287493>
- Töpfer, J., Goodenough, J. B., "Transport and Magnetic Properties of the Perovskites  $\text{La}_{1-y}\text{MnO}_3$  and  $\text{LaMn}_{1-z}\text{O}_3$ ", *Chemistry of Materials*, Vol. 9, No. 6, (1997), 1467-1474. <https://doi.org/10.1021/cm9700211>
- Chandra, S., Biswas, A., Datta, S., Ghosh, B., Siruguri, V., Raychaudhuri, A. K., Phan, M. H., Srikanth, H., "Evidence of a canted magnetic state in self-doped  $\text{LaMnO}_{3+\delta}$  ( $\delta=0.04$ ): a magnetocaloric study", *Journal of Physics: Condensed Matter*, Vol. 24, No. 36, (2012), 366004. <https://doi.org/10.1088/0953-8984/24/36/366004>
- Zener, C., "Interaction between the d-shells in the transition metals. II. Ferromagnetic compounds of manganese with perovskite structure", *Physical Review*, Vol. 82, No. 3, (1951), 403. <https://doi.org/10.1103/PhysRev.82.403>
- Anderson, P. W., Hasegawa, H., "Considerations on double exchange", *Physical Review*, Vol. 100, No. 2, (1955), 675. <https://doi.org/10.1103/PhysRev.100.675>
- De Gennes, P. G., "Effects of double exchange in magnetic crystals", *Physical Review*, Vol. 118, No. 1, (1960), 141. <https://doi.org/10.1103/PhysRev.118.141>
- Malavasi, L., Mozzati, M. C., Azzoni, C. B., Chiodelli, G., Flor, G., "Role of oxygen content on the transport and magnetic properties of  $\text{La}_{1-x}\text{Ca}_x\text{MnO}_{3+\delta}$  manganites", *Solid State communications*, Vol. 123, No. 8, (2002), 321-326. [https://doi.org/10.1016/S0038-1098\(02\)00376-9](https://doi.org/10.1016/S0038-1098(02)00376-9)
- Maguire, E. T., Coats, A. M., Skakle, J. M., West, A. R., "Stoichiometry and defect structure of  $\text{NdMnO}_3$ ", *Journal of Materials Chemistry*, Vol. 9, No. 6, (1999), 1337-1346. <https://doi.org/10.1039/a900734b>
- Dagotto, E., "Phase Diagrams and Basic Properties of Manganites", In *Nanoscale Phase Separation and Colossal Magnetoresistance*, Springer Series in Solid-State Sciences, vol

136. Springer, Berlin, Heidelberg. [https://doi.org/10.1007/978-3-662-05244-0\\_3](https://doi.org/10.1007/978-3-662-05244-0_3)
12. Wollan, E. O., Koehler, W. C., "Neutron diffraction study of the magnetic properties of the series of perovskite-type Compounds  $[(1-x)\text{La}, x\text{Ca}]\text{MnO}_3$ ", *Physical Review*, Vol. 100, No. 2, (1955), 545. <https://doi.org/10.1103/PhysRev.100.545>
  13. Kagan, M. Y., Klaptsov, A. V., Brodsky, I. V., Kugel, K. I., Sboychakov, A. O., Rakhmanov, A. L., "Nanoscale phase separation in manganites", *Journal of Physics A: Mathematical and General*, Vol. 36, No. 35, (2003), 9155. <https://doi.org/10.1088/0305-4470/36/35/304>
  14. Hwang, H. Y., Cheong, S. W., Radaelli, P. G., "Lattice Effects on the Magnetoresistance in Doped  $\text{LaMnO}_3$ ", *Physical Review Letters*, Vol. 75, No. 5, (1995), 914. <https://doi.org/10.1103/PhysRevLett.75.914>
  15. Zariifi, M., Kameli, P., Ehsani, M. H., Ahmadvand, H., Salamati, H., "Effects of rare earth ions substitution on the magnetocaloric and critical behavior of  $\text{La}_{0.6}\text{A}_{0.2}\text{Sr}_{0.2}\text{MnO}_3$  (A= Pr, Nd, Ce) manganite", *Journal of Alloys and Compounds*, Vol. 718, (2017), 443-452. <https://doi.org/10.1016/j.jallcom.2017.05.196>
  16. Arabi, A., Fazli, M., Ehsani, M. H., "Tuning the morphology and photocatalytic activity of  $\text{La}_{0.7}\text{Ca}_{0.3}\text{MnO}_3$  nanorods via different mineralizer-assisted hydrothermal syntheses", *Materials Research Bulletin*, Vol. 90, (2017), 205-211. <https://doi.org/10.1016/j.materresbull.2017.02.043>
  17. Zariifi, M., Kameli, P., Ehsani, M. H., Ahmadvand, H., Salamati, H., "Effects of strain on the magnetic and transport properties of the epitaxial  $\text{La}_{0.5}\text{Ca}_{0.5}\text{MnO}_3$  thin films", *Journal of Magnetism and Magnetic Materials*, Vol. 420, (2016), 33-38. <https://doi.org/10.1016/j.jmmm.2016.06.081>
  18. Ehsani, M. H., Raoufi, T., Razavi, F. S., "Impact of Gd ion substitution on the magneto-caloric effect of  $\text{La}_{0.6-x}\text{Gd}_x\text{Sr}_{0.4}\text{MnO}_3$  ( $x=0, 0.0125, 0.05, 0.10$ ) manganites", *Journal of Magnetism and Magnetic Materials*, Vol. 475, (2019), 484-492. <https://doi.org/10.1016/j.jmmm.2018.11.131>
  19. Ehsani, M. H., Raoufi, T., "Effect of Gd substitution on the critical scaling of the ferromagnetic transition of  $\text{La}_{0.6-x}\text{Gd}_x\text{Sr}_{0.4}\text{MnO}_3$  ( $x=0, 0.05, 0.1$ ) manganite", *Journal of Alloys and Compounds*, Vol. 769, (2018), 649-659. <https://doi.org/10.1016/j.jallcom.2018.08.022>
  20. Esmaeili, S., Ehsani, M. H., Fazli, M., "Photo-catalytic activities of  $\text{La}_{0.7}\text{Ba}_{0.3}\text{MnO}_3$  nanoparticles", *Optik*, Vol. 216, (2020), 164812. <https://doi.org/10.1016/j.ijleo.2020.164812>
  21. Esmaeili, S., Ehsani, M. H., Fazli, M., "Structural, optical and photocatalytic properties of  $\text{La}_{0.7}\text{Ba}_{0.3}\text{MnO}_3$  nanoparticles prepared by microwave method", *Chemical Physics*, Vol. 529, (2020), 110576. <https://doi.org/10.1016/j.chemphys.2019.110576>
  22. De Lima, O. F., Coaquira, J. A. H., De Almeida, R. L., De Carvalho, L. B., Malik, S. K., "Magnetic phase evolution in the  $\text{LaMn}_{1-x}\text{Fe}_x\text{O}_{3+y}$  system", *Journal of Applied Physics*, Vol. 105, No. 1, (2009), 013907. <https://doi.org/10.1063/1.3054323>
  23. Sun, Y., Tong, W., Xu, X., Zhang, Y., "Possible double-exchange interaction between manganese and chromium in  $\text{LaMn}_{1-x}\text{Cr}_x\text{O}_3$ ", *Physical Review B*, Vol. 63, No. 17, (2001), 174438. <https://doi.org/10.1103/PhysRevB.63.174438>
  24. Ramos, A. Y., Tolentino, H. C., Soares, M. M., Grenier, S., Bunãu, O., Joly, Y., Baudalet, F., Wilhelm, F., Rogalev, A., Souza, R. A., Souza-Neto, N. M., "Emergence of ferromagnetism and Jahn-Teller distortion in  $\text{LaMn}_{1-x}\text{Cr}_x\text{O}_3$  ( $x<0.15$ )", *Physical Review B*, Vol. 87, No. 22, (2013), 220404. <https://doi.org/10.1103/PhysRevB.87.220404>
  25. Gong, F., Tong, W., Tan, S., Zhang, Y., "Large effect of small Zn doping on the electric and magnetic properties in  $\text{LaMn}_{1-x}\text{Zn}_x\text{O}_3$ ", *Physical Review B*, Vol. 68, No. 17, (2003), 174410. <https://doi.org/10.1103/PhysRevB.68.174410>
  26. Hu, L., Tong, W., Zhu, H., Zhang, Y., "The effects of Jahn-Teller distortion changes on transport properties in  $\text{LaMn}_{1-x}\text{Zn}_x\text{O}_3$ ", *Journal of Physics: Condensed Matter*, Vol. 15, No. 12, (2003), 2033. <https://doi.org/10.1088/0953-8984/15/12/320>
  27. Sahana, M., Venimadhav, A., Hegde, M. S., Nenkov, K., Rößler, U. K., Dörr, K., Müller, K. H., "Magnetic properties and specific heat of  $\text{LaMn}_{1-x}\text{Ti}_x\text{O}_{3+\delta}$  ( $0<x\leq 0.2$ )", *Journal of Magnetism and Magnetic Materials*, Vol. 260, No. 3, (2003), 361-370. [https://doi.org/10.1016/S0304-8853\(02\)01341-0](https://doi.org/10.1016/S0304-8853(02)01341-0)
  28. Hébert, S., Martin, C., Maignan, A., Retoux, R., Hervieu, M., Nguyen, N., Raveau, B., "Induced ferromagnetism in  $\text{LaMnO}_3$  by Mn-site substitution: The major role of Mn mixed valency", *Physical Review B*, Vol. 65, No. 10, (2002), 104420. <https://doi.org/10.1103/PhysRevB.65.104420>
  29. Sun, Y., Xu, X., Tong, W., Zhang, Y., "Double-exchange ferromagnetism and magnetoresistance in  $\text{LaMn}_{1-x}\text{Cu}_x\text{O}_3$  ( $x\leq 0.3$ )", *Applied Physics Letters*, Vol. 77, No. 17, (2000), 2734-2736. <https://doi.org/10.1063/1.1320021>
  30. Michel, C., "Structural, electro-magnetic and catalytic characterisation of the  $\text{LaMn}_{1-x}\text{Cu}_x\text{O}_{3-\delta}$  system", *Journal of Material Chemistry*, Vol. 8, No. 8, (1998), 1815-1819. <https://doi.org/10.1039/a801503a>
  31. Eshraghi, M., Kameli, P., Khalili, F., Ehsani, M. H., Salamati, H., "Structural, magnetic and electrical characterization of the  $\text{La}_{0.7}\text{Ca}_{0.3}\text{Co}_{1-x}\text{Mn}_x\text{O}_3$  ( $x=0, 0.7$  and  $1$ ) compounds prepared by a simple method", *Journal of Rare Earths*, Vol. 32, No. 10, (2014), 965-972. [https://doi.org/10.1016/s1002-0721\(14\)60170-8](https://doi.org/10.1016/s1002-0721(14)60170-8)
  32. Amirzadeh, P., Ahmadvand, H., Kameli, P., Aslibeiki, B., Salamati, H., Gamzatov, A. G., Aliev, A. M., Kamilov, I. K., "Phase separation and direct magnetocaloric effect in  $\text{La}_{0.5}\text{Ca}_{0.5}\text{MnO}_3$  manganite", *Journal of Applied Physics*, Vol. 113, No. 12, (2013), 123904. <https://doi.org/10.1063/1.4794179>
  33. Joy, P. A., Sankar, C. R., Date, S. K., "The origin of ferromagnetism in  $\text{LaMnO}_{3+\delta}$ ", *Journal of Physics: Condensed Matter*, Vol. 14, No. 19, (2002), 4985. <https://doi.org/10.1088/0953-8984/14/19/320>
  34. Zhang, H., Shi, J., Li, Y., Liu, H., Dong, X., Chen, K., Hou, Q., Huang, Y., Ge, X., Zhao, L., Lu, Z., "Local Atomic and Electronic Structure with Magnetism of  $\text{La}_{0.7}\text{Ca}_{0.3}\text{Mn}_{1-x}\text{Cu}_x\text{O}_3$  ( $x=0, 0.03, 0.06, 0.1$ )", *Journal of Low Temperature Physics*, Vol. 169, No. 1-2, (2012), 77-89. <https://doi.org/10.1007/s10909-012-0644-1>
  35. Shannon, R. D., "Revised effective ionic radii and systematic studies of interatomic distances in halides and chalcogenides", *Acta Crystallographica Section A: Crystal Physics, Diffraction, Theoretical and General Crystallography*, Vol. 32, No. 5, (1976), 751-767. <https://doi.org/10.1107/s0567739476001551>
  36. Yuan, S. L., Jiang, Y., Li, G., Li, J. Q., Yang, Y. P., Zeng, X. Y., Tang, P., Huang, Z., "Semiconductor-metal transition and magnetoresistance in  $\text{La}_{(1+x)/3}\text{Ba}_{(2-x)/3}\text{Cu}_{1-x}\text{Mn}_x\text{O}_3$ ", *Physical Review B*, Vol. 61, No. 5, (2000), 3211. <https://doi.org/10.1103/physrevb.61.3211>
  37. Kim, M. S., Yang, J. B., Medvedeva, J., Yelon, W. B., Parris, P. E., James, W. J., "Electronic structure of  $\text{La}_{0.7}\text{Sr}_{0.3}\text{Mn}_{1-x}\text{Cu}_x\text{O}_3$  ( $0.0\leq x\leq 0.30$ )", *Journal of Physics: Condensed Matter*, Vol. 20, No. 25, (2008), 255228. <https://doi.org/10.1088/0953-8984/20/25/255228>
  38. Töpfer, J., Goodenough, J. B., "LaMnO<sub>3+δ</sub> Revisited", *Journal of Solid State Chemistry*, Vol. 130, No. 1, (1997), 117-128. <https://doi.org/10.1006/jssc.1997.7287>
  39. Aslibeiki, B., Kameli, P., Salamati, H., "Reentrant spin glass behavior in  $\text{La}_{0.8}\text{Sr}_{0.2}\text{Mn}_{1-x}\text{Ti}_x\text{O}_3$  manganites", *Solid State Communications*, Vol. 149, No. 31-32, (2009), 1274-1277. <https://doi.org/10.1016/j.ssc.2009.05.012>
  40. Pękala, M., Mucha, J., Vertruyen, B., Cloots, R., Ausloos, M., "Effect of Ga doping on magneto-transport properties in colossal magnetoresistive  $\text{La}_{0.7}\text{Ca}_{0.3}\text{Mn}_{1-x}\text{Ga}_x\text{O}_3$  ( $0<x<0.1$ )", *Journal of*

- Magnetism and Magnetic Materials*, Vol. 306, No. 2, (2006), 181-190. <https://doi.org/10.1016/j.jmmm.2006.02.241>
41. Dho, J., Kim, W. S., Hur, N. H., "Reentrant spin glass behavior in Cr-doped perovskite manganite", *Physical Review Letters*, Vol. 89, No. 2, (2002), 027202. <https://doi.org/10.1103/physrevlett.89.027202>
  42. Srivastava, S. K., Kar, M., Ravi, S., "Ferromagnetic insulating and spin glass behavior in Cr substituted  $\text{La}_{0.85}\text{Ag}_{0.15}\text{MnO}_3$  compounds", *Journal of Physics: Condensed Matter*, Vol. 20, No. 23, (2008), 235201. <https://doi.org/10.1088/0953-8984/20/23/235201>
  43. Viswanathan, M., Kumar, P. A., "Observation of reentrant spin glass behavior in  $\text{LaCo}_{0.5}\text{Ni}_{0.5}\text{O}_3$ ", *Physical Review B*, Vol. 80, No. 1, (2009), 012410. <https://doi.org/10.1103/physrevb.80.012410>
  44. Mydosh, J. A., *Spin Glasses: An Experimental Introduction*, Taylor and Francis, (1993). <https://doi.org/10.1201/9781482295191>
  45. Pi, L., Zheng, L., Zhang, Y., "Transport mechanism in polycrystalline  $\text{La}_{0.825}\text{Sr}_{0.175}\text{Mn}_{1-x}\text{Cu}_x\text{O}_3$ ", *Physical Review B*, Vol. 61, No. 13, (2000), 8917. <https://doi.org/10.1103/physrevb.61.8917>
  46. Banerjee, A., Pal, S., Chaudhuri, B. K., "Nature of small-polaron hopping conduction and the effect of Cr doping on the transport properties of rare-earth manganite  $\text{La}_{0.5}\text{Pb}_{0.5}\text{Mn}_{1-x}\text{Cr}_x\text{O}_3$ ", *The Journal of Chemical Physics*, Vol. 115, No. 3, (2001), 1550-1558. <https://doi.org/10.1063/1.1378018>
  47. Mott, N. F., "Conduction in glasses containing transition metal ions", *Journal of Non-Crystalline Solids*, Vol. 1, No. 1, (1968), 1-17. [https://doi.org/10.1016/0022-3093\(68\)90002-1](https://doi.org/10.1016/0022-3093(68)90002-1)
  48. Ravi, S., Kar, M., "Study of magneto-resistivity in  $\text{La}_{1-x}\text{Ag}_x\text{MnO}_3$  compounds", *Physica B: Condensed Matter*, Vol. 348, No. 1-4, (2004), 169-176. <https://doi.org/10.1016/j.physb.2003.11.087>
  49. Emin, D., Holstein, T., "Studies of small-polaron motion IV. Adiabatic theory of the Hall effect", *Annals of Physics*, Vol. 53, No. 3, (1969), 439-520. [https://doi.org/10.1016/0003-4916\(69\)90034-7](https://doi.org/10.1016/0003-4916(69)90034-7)
  50. Holstein, T., "Theory of transport phenomena in an electron-phonon gas", *Annals of Physics*, Vol. 29, No. 3, (1964), 410-535. [https://doi.org/10.1016/0003-4916\(64\)90008-9](https://doi.org/10.1016/0003-4916(64)90008-9)
  51. Mollah, S., Khan, Z. A., Shukla, D. K., Arshad, M., Kumar, R., Das, A., "Adiabatic small polaron-hopping conduction in  $\text{Ln}_{0.85}\text{Ca}_{0.15}\text{MnO}_3$  (Ln= Nd, Pr and Sm) perovskites", *Journal of Physics and Chemistry of Solids*, Vol. 69, No. 4, (2008), 1023-1028. <https://doi.org/10.1016/j.jpccs.2007.11.024>
  52. Ehsani, M. H., Kameli, P., Ghazi, M. E., "Influence of grain size on the electrical properties of the double-layered  $\text{LaSr}_2\text{Mn}_2\text{O}_7$  manganite", *Journal of Physics and Chemistry of Solids*, Vol. 73, No. 6, (2012), 744-750. <https://doi.org/10.1016/j.jpccs.2012.01.020>
  53. Mansuri, I., Varshney, D., Kaurav, N., Lu, C. L., Kuo, Y. K., "Effects of A-site disorder on magnetic, electrical and thermal properties of  $\text{La}_{0.5-x}\text{Ln}_x\text{Ca}_{0.5-y}\text{Sr}_y\text{MnO}_3$  manganites", *Journal of Magnetism and Magnetic Materials*, Vol. 323, No. 3-4, (2011), 316-323. <https://doi.org/10.1016/j.jmmm.2010.09.026>
  54. Banerjee, A., Pal, S., Rozenberg, E., Chaudhuri, B. K., "Adiabatic and non-adiabatic hopping conduction in La-Pb-Mn-O type system", *Journal of Alloys and Compounds*, Vol. 326, No. 1-2, (2001), 85-88. [https://doi.org/10.1016/s0925-8388\(01\)01229-4](https://doi.org/10.1016/s0925-8388(01)01229-4)
  55. Austin, I. G., Mott, N. F., "Polarons in crystalline and non-crystalline materials", *Advances in Physics*, Vol. 18, No. 71, (1969), 41-102. <https://doi.org/10.1080/00018736900101267>